Cell Stem Cell, Volume *20*

Supplemental Information

Human iPSC-Derived Neural Progenitors Are an Effective Drug Discovery Model for Neurological mtDNA Disorders

Carmen Lorenz, Pierre Lesimple, Raul Bukowiecki, Annika Zink, Gizem Inak, Barbara Mlody, Manvendra Singh, Marcus Semtner, Nancy Mah, Karine Auré, Megan Leong, Oleksandr Zabiegalov, Ekaterini-Maria Lyras, Vanessa Pfiffer, Beatrix Fauler, Jenny Eichhorst, Burkhard Wiesner, Norbert Huebner, Josef Priller, Thorsten Mielke, David Meierhofer, Zsuzsanna Izsvák, Jochen C. Meier, Frédéric Bouillaud, James Adjaye, Markus Schuelke, Erich E. Wanker, Anne Lombès, and Alessandro Prigione

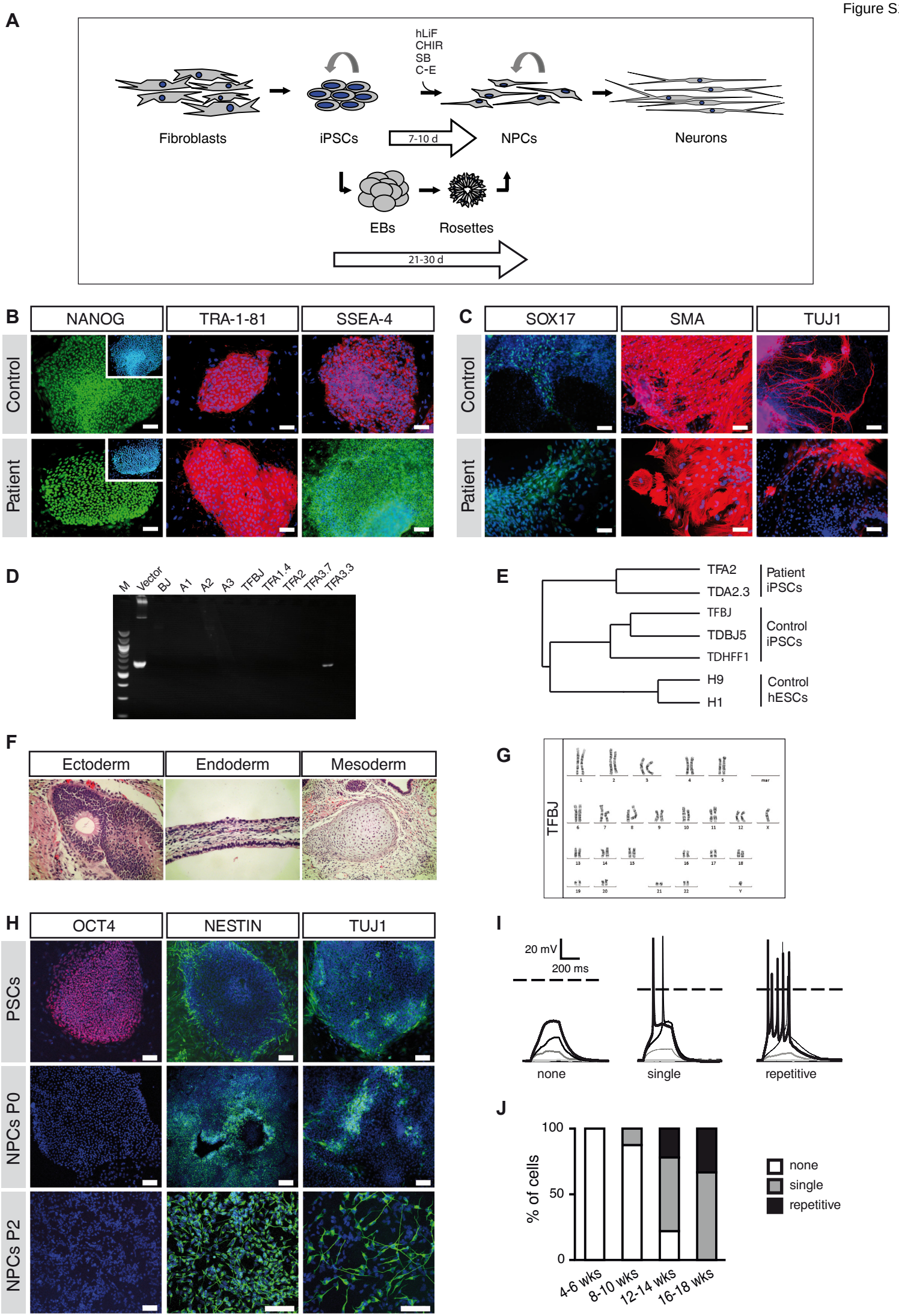
A
hLiF
CHIR
SB
C-E
Fibroblasts
iPSCs
7-10 d
NPCs
Neurons
EBs
Rosettes
21-30 d
B
NANOG
TRA-1-81
SSEA-4
Control
Patient
C
SOX17
SMA
TUJ1
Control
Patient
D
M
Vector
BJ
A1
A2
A3
TFBJ
TFA1.4
TFA2
TFA3.7
TFA3.3
E
TFA2
TDA2.3
Patient iPSCs
TFBJ
TDBJ5
TDHFF1
Control iPSCs
H9
H1
Control hESCs
F
Ectoderm
Endoderm
Mesoderm
G
TFBJ
H
OCT4
NESTIN
TUJ1
PSCs
NPCs P0
NPCs P2
I
20 mV
200 ms
none
single
repetitive
J
100
50
0
% of cells
4-6 wks
8-10 wks
12-14 wks
16-18 wks
none
single
repetitive

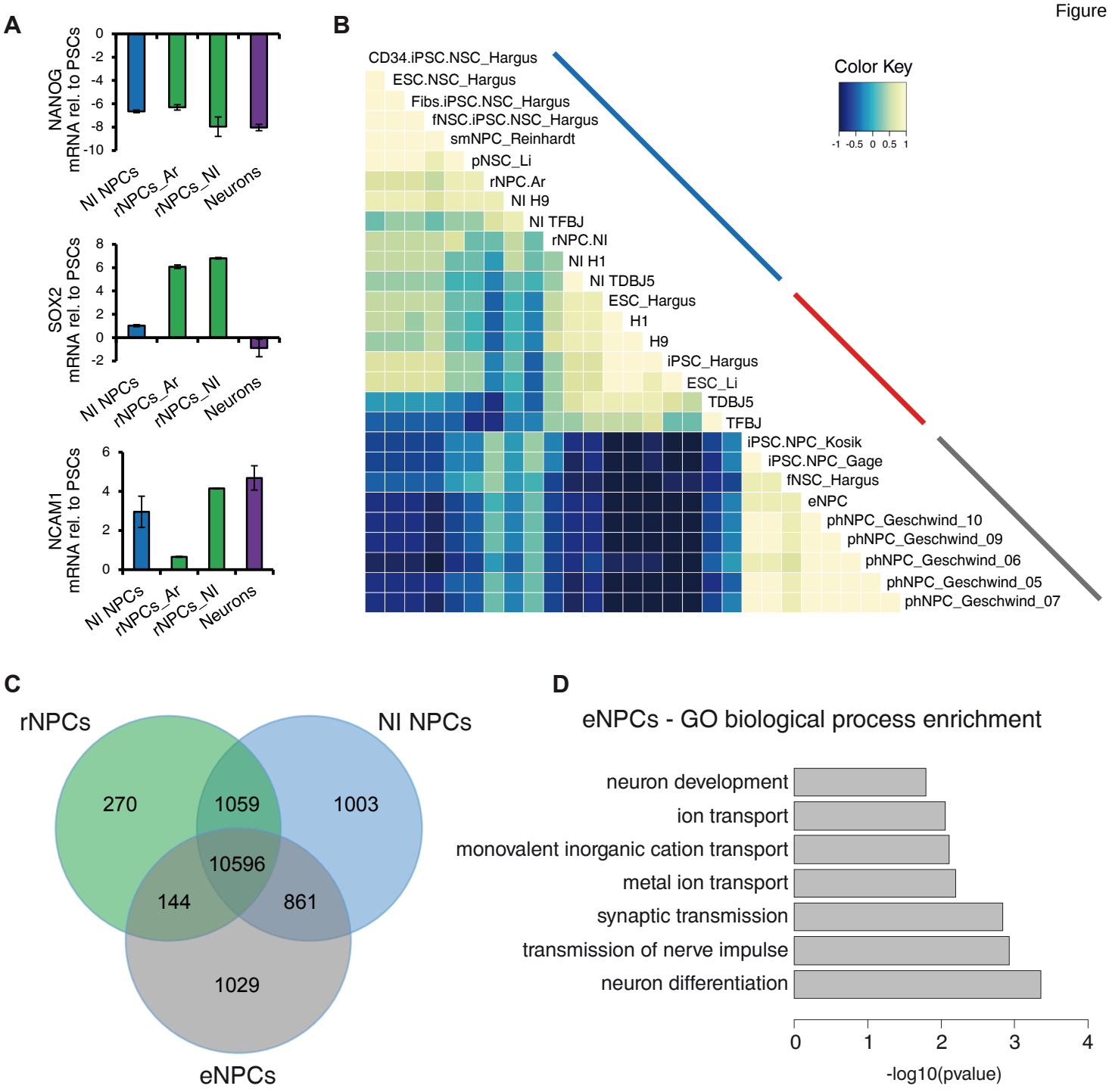
A
NANOG mRNA rel. to PSCs
SOX2 mRNA rel. to PSCs
NCAM1 mRNA rel. to PSCs
NI NPCs
rNPCs_Ar
rNPCs_NI
Neurons
B
Color Key
CD34.iPSC.NSC_Hargus
ESC.NSC_Hargus
Fibs.iPSC.NSC_Hargus
fNSC.iPSC.NSC_Hargus
smNPC_Reinhardt
pNSC_Li
rNPC.Ar
NI H9
NI TFBJ
rNPC.NI
NI H1
NI TDBJ5
ESC_Hargus
H1
H9
iPSC_Hargus
ESC_Li
TDBJ5
TFBJ
iPSC.NPC_Kosik
iPSC.NPC_Gage
fNSC_Hargus
eNPC
phNPC_Geschwind_10
phNPC_Geschwind_09
phNPC_Geschwind_06
phNPC_Geschwind_05
phNPC_Geschwind_07
C
rNPCs
NI NPCs
eNPCs
270
1059
1003
10596
144
861
1029
D
eNPCs - GO biological process enrichment
neuron development
ion transport
monovalent inorganic cation transport
metal ion transport
synaptic transmission
transmission of nerve impulse
neuron differentiation
-log10(pvalue)
E
Basal respiration OCR [(pmol/min)/DNA]
F
Max. respiration OCR [(pmol/min)/DNA]
**
G
Proton leak OCR [(pmol/min)/DNA]
PSCs
Fibroblasts
NPCs
Neurons

Figure S3

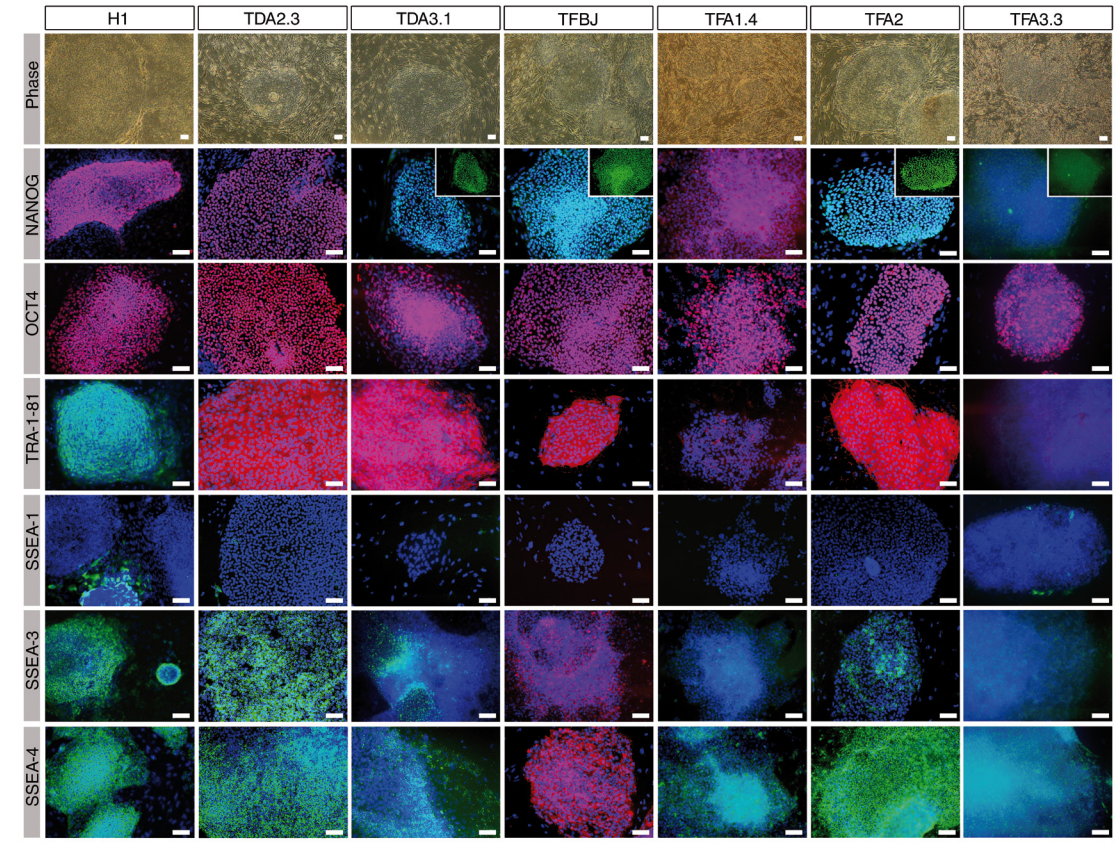
A
H1
TDA2.3
TDA3.1
TFBJ
TFA1.4
TFA2
TFA3.3
Phase
NANOG
OCT4
TRA-1-81
SSEA-1
SSEA-3
SSEA-4

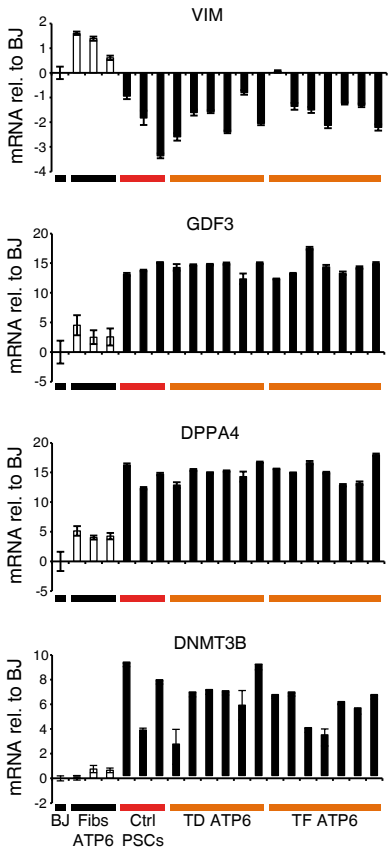
B
VIM
GDF3
DPPA4
DNMT3B
mRNA rel. to BJ
BJ
Fibs ATP6
Ctrl PSCs
TD ATP6
TF ATP6

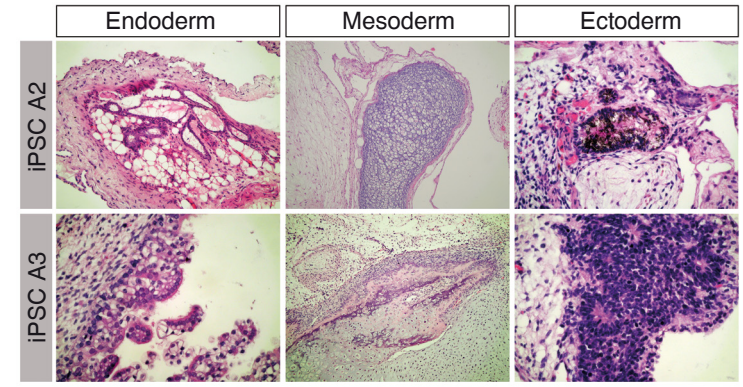
C
Endoderm
Mesoderm
Ectoderm
iPSC A2
iPSC A3

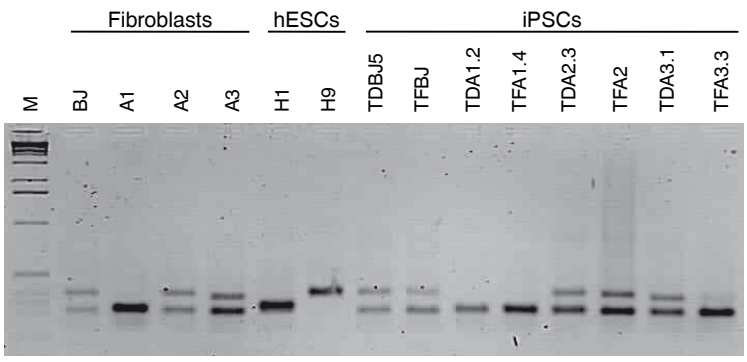
D
Fibroblasts
hESCs
iPSCs
M
BJ
A1
A2
A3
H1
H9
TDBJ5
TFBJ
TDA1.2
TFA1.4
TDA2.3
TFA2
TDA3.1
TFA3.3

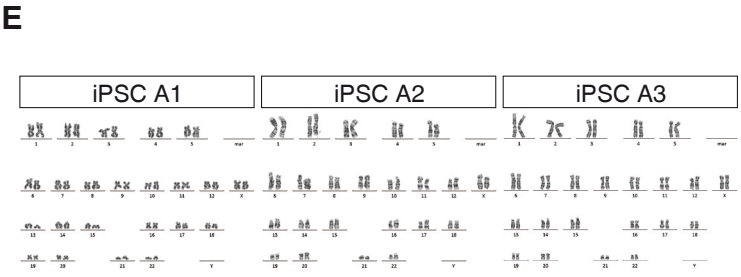
E
iPSC A1
iPSC A2
iPSC A3

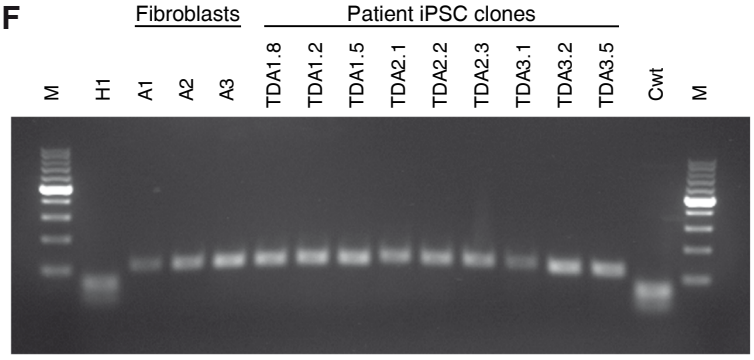
F
Fibroblasts
Patient iPSC clones
M
H1
A1
A2
A3
TDA1.8
TDA1.2
TDA1.5
TDA2.1
TDA2.2
TDA2.3
TDA3.1
TDA3.2
TDA3.5
Cwt
M

A

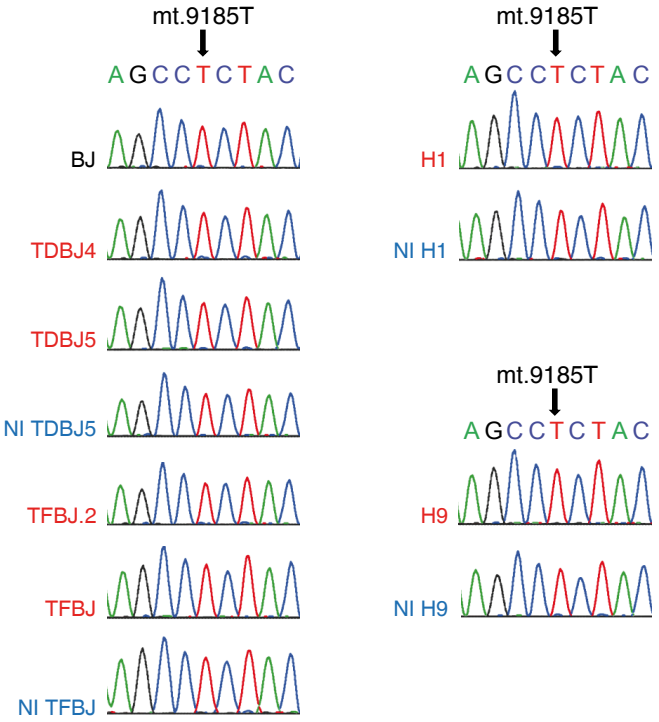

B

Patient	A2	A3
Total number of mtDNA variants	18	17
Disease-associated	1	1
D-loop	9	10
mRNA	6	3
tRNA	0	0
rRNA	3	4
Homoplasmic	17	16
Heteroplasmic	1	1
Acquired in iPSCs (%)	*0*	*0*
Retained in iPSCs (%)	*100*	*100*
Acquired in NPCs (%)	*0*	*0*
Retained in NPCs (%)	*100*	*100*

C

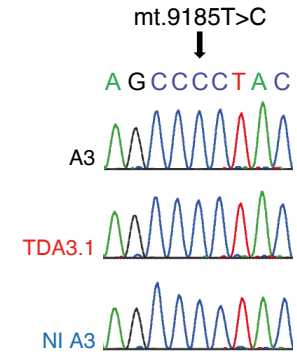

D

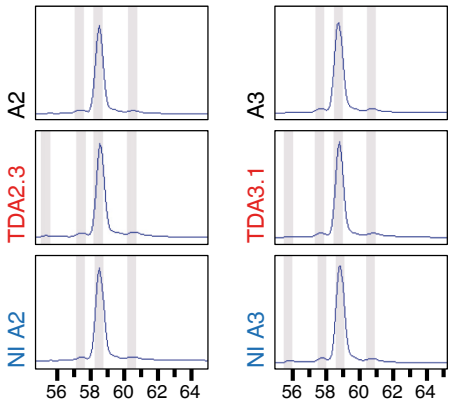

E

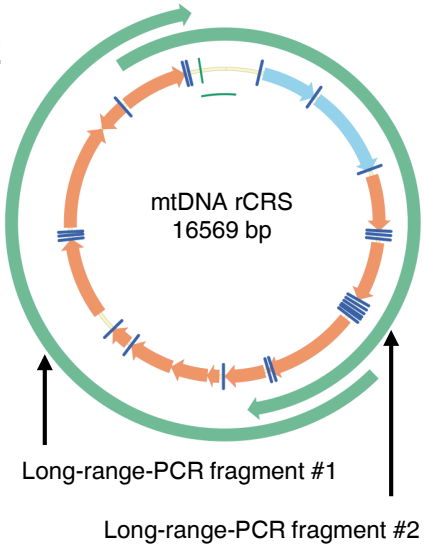

F

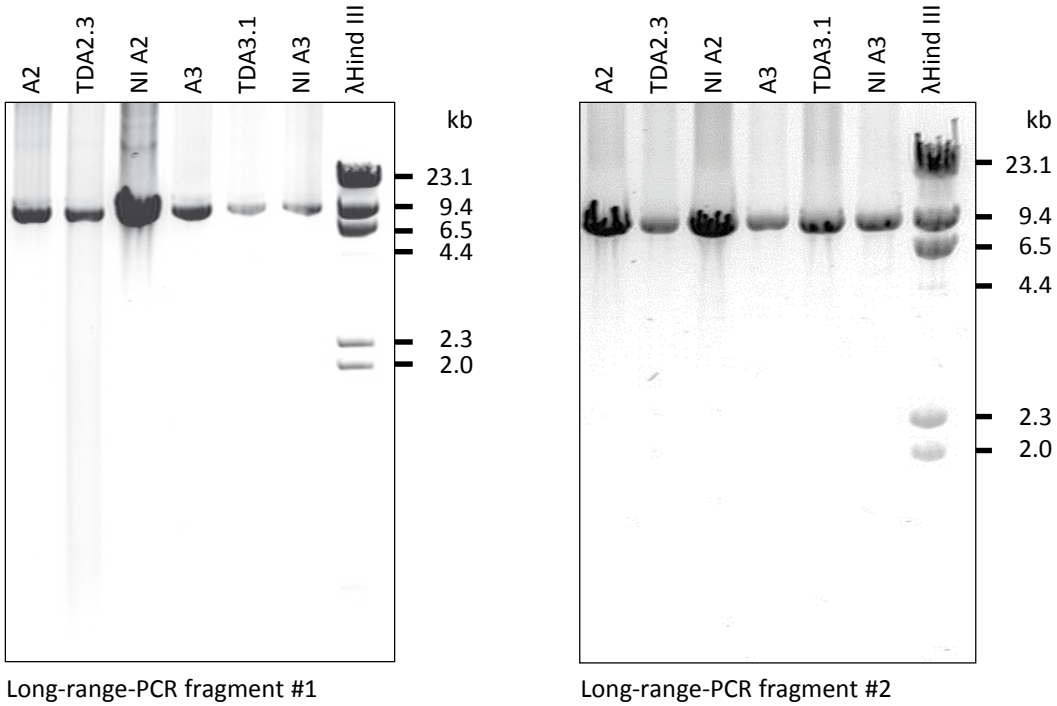

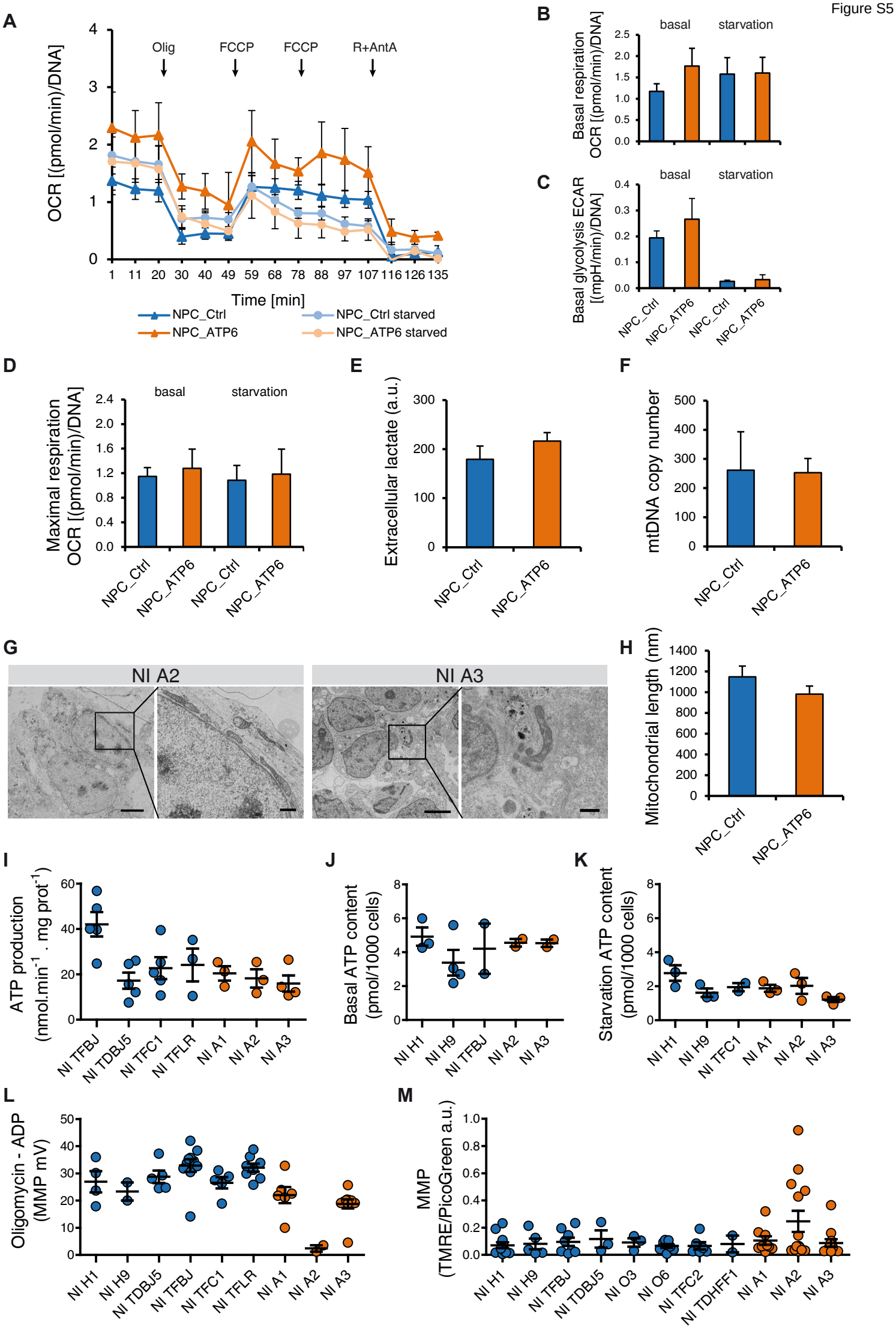
A
OCR [(pmol/min)/DNA]
Olig
FCCP
FCCP
R+AntA
Time [min]
NPC_Ctrl
NPC_ATP6
NPC_Ctrl starved
NPC_ATP6 starved
B
Basal respiration OCR [(pmol/min)/DNA]
basal
starvation
C
Basal glycolysis ECAR [(mpH/min)/DNA]
basal
starvation
NPC_Ctrl
NPC_ATP6
NPC_Ctrl
NPC_ATP6
D
Maximal respiration OCR [(pmol/min)/DNA]
basal
starvation
NPC_Ctrl
NPC_ATP6
NPC_Ctrl
NPC_ATP6
E
Extracellular lactate (a.u.)
NPC_Ctrl
NPC_ATP6
F
mtDNA copy number
NPC_Ctrl
NPC_ATP6
G
NI A2
NI A3
H
Mitochondrial length (nm)
NPC_Ctrl
NPC_ATP6
I
ATP production (nmol.min-1 . mg prot-1)
NI TFBJ
NI TDBJ5
NI TFC1
NI TFLR
NI A1
NI A2
NI A3
J
Basal ATP content (pmol/1000 cells)
NI H1
NI H9
NI TFBJ
NI A2
NI A3
K
Starvation ATP content (pmol/1000 cells)
NI H1
NI H9
NI TFC1
NI A1
NI A2
NI A3
L
Oligomycin - ADP (MMP mV)
NI H1
NI H9
NI TDBJ5
NI TFBJ
NI TFC1
NI TFLR
NI A1
NI A2
NI A3
M
MMP (TMRE/PicoGreen a.u.)
NI H1
NI H9
NI TFBJ
NI TDBJ5
NI O3
NI O6
NI TFC2
NI TDHFF1
NI A1
NI A2
NI A3

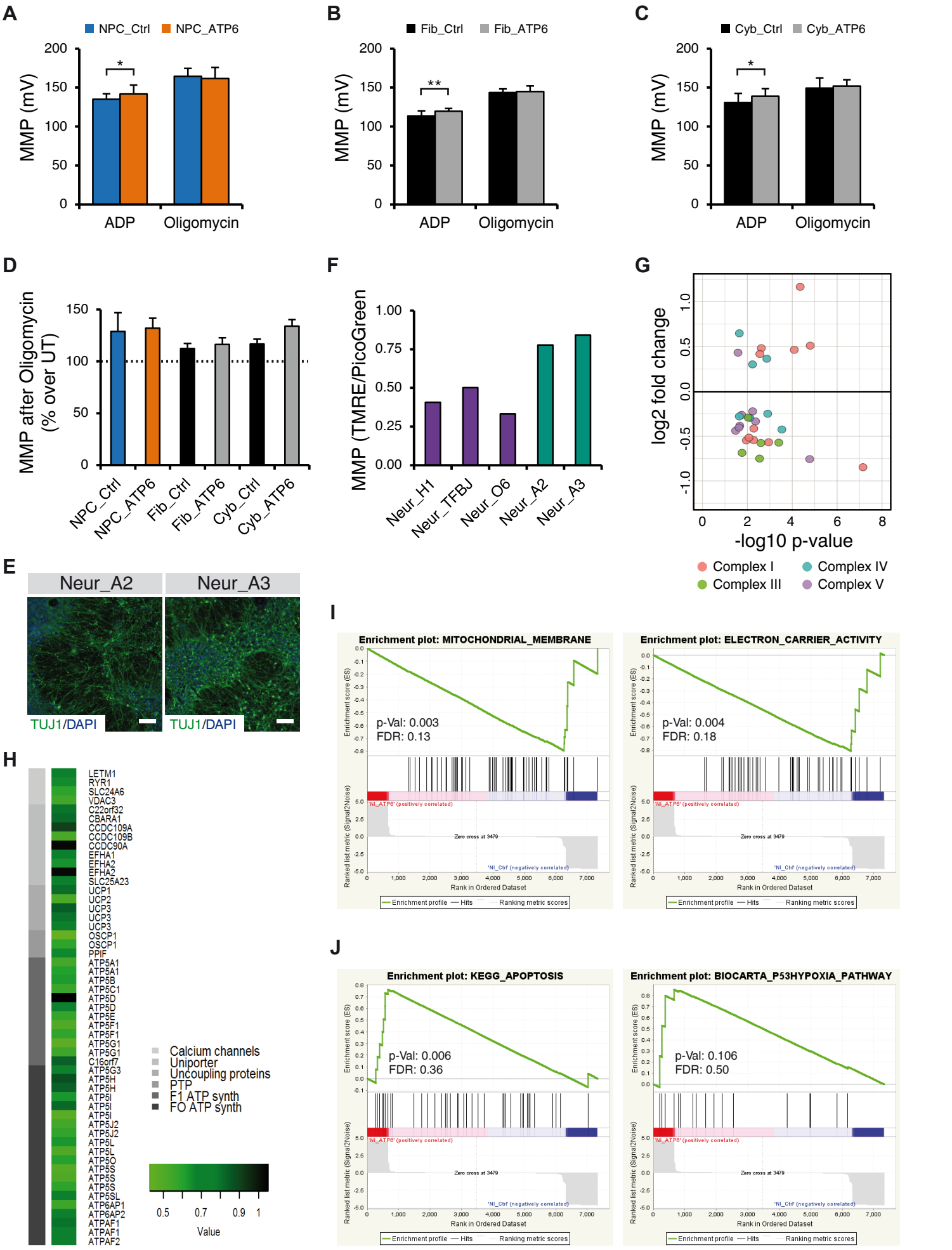
A
NPC_Ctrl
NPC_ATP6
MMP (mV)
ADP
Oligomycin
B
Fib_Ctrl
Fib_ATP6
C
Cyb_Ctrl
Cyb_ATP6
D
MMP after Oligomycin (% over UT)
NPC_Ctrl
NPC_ATP6
Fib_Ctrl
Fib_ATP6
Cyb_Ctrl
Cyb_ATP6
F
MMP (TMRE/PicoGreen
Neur_H1
Neur_TFBJ
Neur_O6
Neur_A2
Neur_A3
G
log2 fold change
-log10 p-value
Complex I
Complex III
Complex IV
Complex V
E
Neur_A2
Neur_A3
TUJ1/DAPI
TUJ1/DAPI
I
Enrichment plot: MITOCHONDRIAL_MEMBRANE
p-Val: 0.003
FDR: 0.13
Enrichment plot: ELECTRON_CARRIER_ACTIVITY
p-Val: 0.004
FDR: 0.18
Enrichment score (ES)
Ranked list metric (Signal2Noise)
Rank in Ordered Dataset
Enrichment profile
Hits
Ranking metric scores
H
LETM1
RYR1
SLC24A6
VDAC3
C22orf32
CBARA1
CCDC109A
CCDC109B
CCDC90A
EFHA1
EFHA2
EFHA2
SLC25A23
UCP1
UCP2
UCP3
UCP3
UCP3
OSCP1
OSCP1
PPIF
ATP5A1
ATP5A1
ATP5B
ATP5C1
ATP5D
ATP5E
ATP5F1
ATP5F1
ATP5G1
ATP5G1
C16orf7
ATP5G3
ATP5H
ATP5H
ATP5I
ATP5I
ATP5I
ATP5J2
ATP5J2
ATP5L
ATP5L
ATP5O
ATP5S
ATP5S
ATP5S
ATP5SL
ATP6AP1
ATP6AP2
ATPAF1
ATPAF1
ATPAF2
Calcium channels
Uniporter
Uncoupling proteins
PTP
F1 ATP synth
FO ATP synth
Value
J
Enrichment plot: KEGG_APOPTOSIS
p-Val: 0.006
FDR: 0.36
Enrichment plot: BIOCARTA_P53HYPOXIA_PATHWAY
p-Val: 0.106
FDR: 0.50

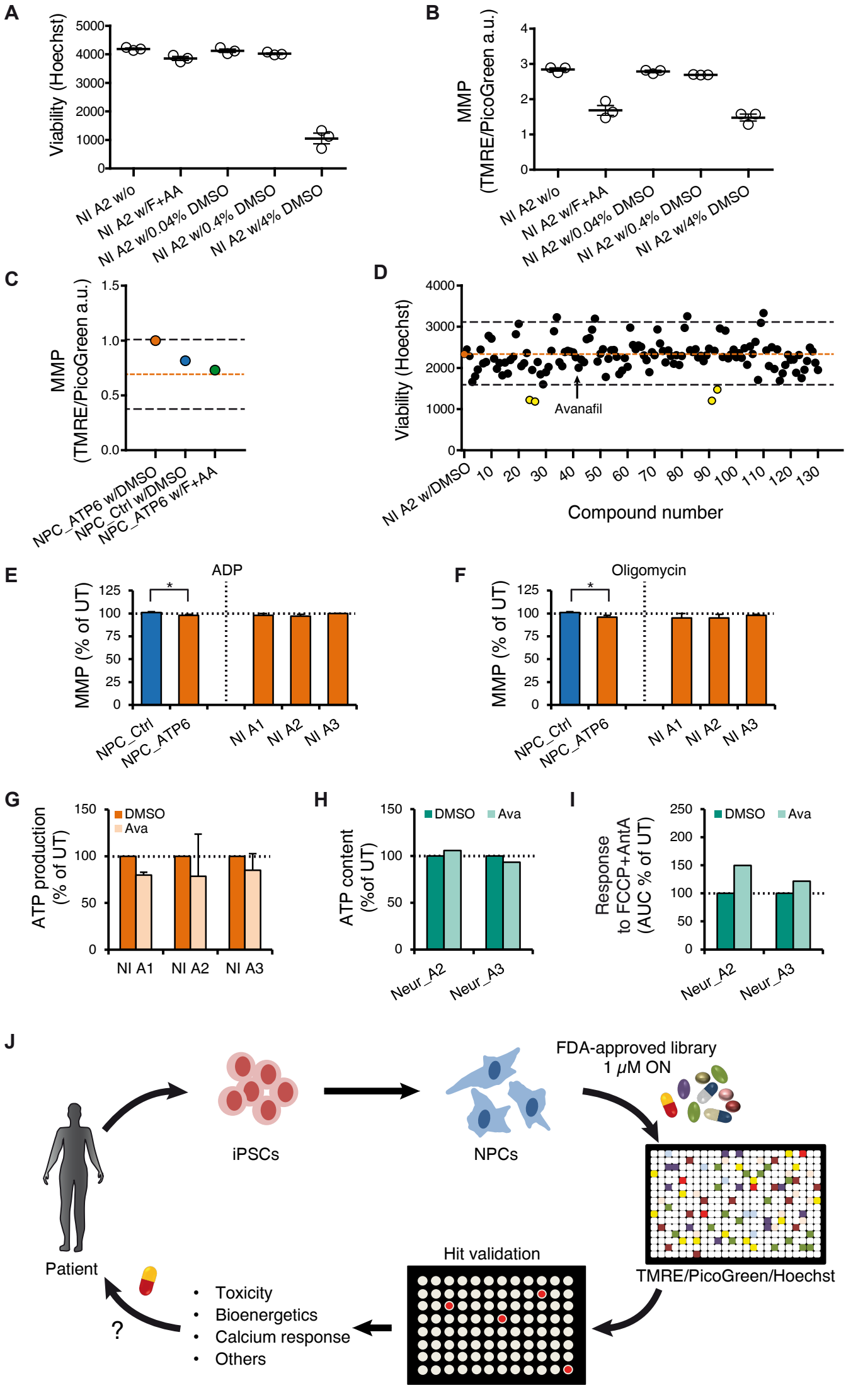
A
Viability (Hoechst)
5000
4000
3000
2000
1000
0
NI A2 w/o
NI A2 w/F+AA
NI A2 w/0.04% DMSO
NI A2 w/0.4% DMSO
NI A2 w/4% DMSO
B
MMP
(TMRE/PicoGreen a.u.)
4
3
2
1
0
NI A2 w/o
NI A2 w/F+AA
NI A2 w/0.04% DMSO
NI A2 w/0.4% DMSO
NI A2 w/4% DMSO
C
MMP
(TMRE/PicoGreen a.u.)
1.5
1.0
0.5
0.0
NPC_ATP6 w/DMSO
NPC_Ctrl w/DMSO
NPC_ATP6 w/F+AA
D
Viability (Hoechst)
4000
3000
2000
1000
0
Avanafil
NI A2 w/DMSO
10
20
30
40
50
60
70
80
90
100
110
120
130
Compound number
E
ADP
MMP (% of UT)
125
100
75
50
25
0
*
NPC_Ctrl
NPC_ATP6
NI A1
NI A2
NI A3
F
Oligomycin
MMP (% of UT)
125
100
75
50
25
0
*
NPC_Ctrl
NPC_ATP6
NI A1
NI A2
NI A3
G
ATP production
(% of UT)
150
100
50
0
DMSO
Ava
NI A1
NI A2
NI A3
H
ATP content
(%of UT)
150
100
50
0
DMSO
Ava
Neur_A2
Neur_A3
I
Response
to FCCP+AntA
(AUC % of UT)
250
200
150
100
50
0
DMSO
Ava
Neur_A2
Neur_A3
J
Patient
iPSCs
NPCs
FDA-approved library
1 μM ON
TMRE/PicoGreen/Hoechst
Hit validation
?
Toxicity
Bioenergetics
Calcium response
Others

Supplemental Figure Legends

S1. Neural induction (NI) and episomal plasmid-based reprogramming. Related to Figure 1.
(A) Scheme of NI NPC generation. The small molecule-based approach (lasting 7-10 days) allows bypassing the time-consuming and operator-dependent process of rosette derivation (lasting 21-30 days). **(B-C)** Transfection (TF) of episomal plasmids into control or patient fibroblasts generated TF-iPSC lines that expressed pluripotency marker proteins (NANOG, TRA1-81, SSEA-4) and were capable to *in vitro* differentiate into the three germ layers: endoderm (SOX17), mesoderm (SMA), and ectoderm (TUJ1). Depicted are lines TFBJ (control) and TFA2 (patient). **(D)** The presence of episomal plasmids was assessed by standard PCR. The TF-iPSC lines exhibiting vector integration (like the line TFA3.9 here represented) were excluded from further analysis. BJ, A1, A2, A3: parental fibroblasts; **(E)** Transcriptional profiling of patient and control iPSCs generated *via* retroviral transduction (TD) or plasmid transfection (TF) demonstrates that the reprogramming protocol does not significantly alter the individual identity. TD-iPSCs and TF-iPSCs from control BJ or from patient A2 clustered together irrespective of their generation method. **(F)** Control iPSC line TFBJ was capable of giving rise to the three germ layers *in vivo* through teratoma formation. **(G)** Karyotype analysis of TFBJ confirmed normal male karyotype. **(H)** Neural induction (NI) from PSCs maintained the cells as monolayer under defined media application (here shown for TFBJ line). PSC markers such as OCT4 (PSCs; upper row) were lost after one week in culture (P0; middle row), while NPC markers like NESTIN and TUJ1 were acquired. Upon subsequent passaging, the cells acquired a spiked morphology with stable marker expression (P2; lower row). **(I)** In neuronal differentiation experiments, cells produced "none", "single", or "repetitive" firing upon depolarization. **(J)** Upon prolonged differentiation *in vitro*, the proportion of single and repetitive firing cells increased steadily, indicating successful maturation of neuronal-like cells in culture.

S2. Global transcriptomics and bioenergetics of NI NPCs. Related to Figure 1 and Figure 2.
(A) qPCR analysis of genes associated with pluripotency (*NANOG*), NPCs (*SOX2*), and all neural cells (*NCAM1*). Samples included NI NPCs (NI H1, NI H9, NI TDBJ5, NI TFBJ), rosette-derived NPCs (rNPCs) grown either with the medium provided by the Aruna company (rNPC_Ar), or with our NI medium (rNPC_NI), and dopaminergic neurons. Data are expressed as a ratio with respect to the undifferentiated hESC line H1. **(B)** Genome-wide correlogram comparing the PSCs and NPCs used in this study to previously published human PSC and NPC datasets. A high degree of correlation was evident among PSCs (red), *in vitro* PSC-derived NPCs (blue), and *ex vivo* NPCs (gray). **(C)** Venn diagram depicting the common and distinct transcriptional signatures of NI NPCs (NI H1, NI H9, NI TDBJ5, NI TFBJ), rosette-derived NPCs (rNPCs), and *ex vivo*-derived NPCs (eNPCs). NI NPCs and rNPCs shared a higher number of transcripts possibly because of their similar *in vitro* PSC origin. **(D)** Biological processes of the genes uniquely expressed by eNPCs and not by NI NPCs or rNPCs comprised categories related to neural development and differentiation, potentially indicating the higher neuronal commitment of NPCs derived from *ex vivo* adult brain. **(E-G)** Seahorse-based assessment of basal respiration, maximal respiration and proton leak of PSCs (H1, H9, TFBJ), fibroblasts (BJ, HFF1), NI NPCs (NI H1, NI H9, NI TFBJ), and neurons (from NI H1 and NI TFBJ) (at least two biological replicates per line, each with at least three technical replicates). In all panels, unless otherwise indicated, error bars represent SEM and p values were determined by unpaired two-tailed Student's t-tests with comparison to PSCs: *P≤0.05, **P≤0.01, ***P≤0.001.

S3. Generation of iPSCs carrying a *MT-ATP6* mutation. Related to Figure 4.
(A) The staining pattern of pluripotency-associated marker proteins in TD- and TF-based ATP6-iPSCs (carrying the m.9185T>C *MT-ATP6* mutation) was comparable to that of control PSCs (like H1 and TFBJ here presented). Scale bar: 100 µm. **(B)** Quantification by qPCR of a fibroblast-associated gene (vimentin, *VIM*) and pluripotency-associated genes (*GDF3*, *DPPA4* and *DNMT3B*) in patient fibroblasts (Fib_ATP6, corresponding to A1, A2, and A3), control PSCs (Ctrl PSCs, including H1, TFBJ, and TDBJ5), patient TD-iPSC clones (TD ATP6) and patient TF-iPSC clones (TF ATP6). Data were normalized to BJ control fibroblasts. **(C)** Representative teratoma analyses of ATP6-iPSC lines. **(D)** Individual identity of the derived lines shown by fingerprinting analysis. **(E)** Normal female karyotype of ATP6-iPSC lines derived from the three patients. **(F)** PCR-based *MnlI* restriction analysis demonstrated the presence of virtually homoplasmic levels of the m.9185T>C *MT-ATP6* mutation in all the iPSC clones generated from the three patient fibroblasts. H1 line and wild-type plasmid vector (Cwt) were used as controls. M indicates the marker.

S4. Mitochondrial genotype of patient-derived NPC_ATP6. Related to Figure 4.
(A) Sanger-based whole mtDNA sequencing showed normal sequence at position 9185 from the control fibroblasts BJ and their derived cell lines (TD-derived iPSCs, TF-derived iPSCs, and related NI NPCs) as well as from the lines H1 and H9. **(B)** Summary of the whole mtDNA sequencing analysis for the patient lines A2 and A3. All mtDNA variants present in the patient fibroblasts were retained during reprogramming and differentiation, while no novel mutations were acquired. **(C)** Sanger sequencing showing the m.9185T>C mutation in A3 fibroblasts and their related iPSCs and NI NPCs. **(D)** GeneScan analysis demonstrating the

preservation of the D310 tract hypervariable region of the D-loop in the patients fibroblasts A2 and A3 and in their related iPSCs and NI NPCs. **(E)** Graphical representation of the two long-range PCR fragments used for searching mtDNA deletions. **(F)** Long-range PCR establishing the absence of large mtDNA deletions in the patient fibroblasts A2 and A3 and their related iPSCs and NI NPCs.

S5. Mitochondrial bioenergetics of NPC_ATP6 cells. Related to Figure 4 and Figure 5.
(A) Oxygen consumption rate (OCR) profile in control and patient NPCs under basal conditions (dark lines) and after 4 hours starvation in a medium deprived of glucose and supplements (bright lines). NPC_Ctrl (NI H1, NI H9, NI TFBJ) and NPC_ATP6 (NI A2, NI A3) were measured in at least four technical replicates per run and in at least two biological repeat runs. **(B-C-D)** Basal mitochondrial respiration, basal glycolysis, and maximal respiration did not differ between control NPC lines (NI H1, NI H9, NI TFBJ) and patient NPC lines (NI A2, NI A3) grown in standard conditions or after starvation. **(E)** Extracellular lactate production in NPC_ATP6 did not differ from that of NPC_Ctrl. Four control NPCs (NI H1, NI H9, NI TFBJ, and NI TFC1) and two patient NPCs (NI A2, NI A3) were used in five biological replicates. **(F)** mtDNA copy number per cell in NPC_Ctrl (NI H9, NI TFBJ, NI TDBJ5) and NPC_ATP6 (NI A1, NI A2, NI A3). **(G)** Representative mitochondrial ultrastructure in the NPC_ATP6 lines NI A2 and NI A3. The overall images were constructed merging single micrographs using TrakEM2 within the FIJI software package (Scale bars overview: 5 µm). The inlays refer to a magnified area (Scale bar: 1 µm). **(H)** Quantification of mitochondrial length in control NPCs (NI H1, NI H9, NI TFBJ) and patient NPCs (NI A2, NI A3) calculated measuring at least 50 distinct mitochondria per line. **(I)** ATP production in individual control and patient NPC lines. Related to Fig. 4D. **(J-K)** ATP content under basal and starvation conditions in individual control and patient NPC lines. Related to Fig. 4E. **(L)** MMP quantification as the difference between state 4 respiration (induced by 1 µM oligomycin) and state 3 respiration (induced by 1 mM ADP) in individual control and patient NPC lines. Related to Fig. 5A. **(M)** Imaging-based MMP quantification in intact cells in individual control and patient NPC lines. Related to Fig. 5B.

S6. MMP assessment and global transcriptomics and proteomics. Related to Figure 5 and Figure 6.
(A-C) MMP quantification in permeabilized cells using the Nernst law to express the potential in mV; ADP= state 3 respiration induced by 1 mM ADP; oligomycin= state 4 respiration induced by 1 µM oligomycin; during state 4 respiration. In the three cell types, state 3 respiration reveals the impact of the ATP6 mutation, which reduces the dissipation of MMP for ATP synthesis and leads to significant increase of MMP. In contrast, the MMP is similar in control and mutant cells during state 4 respiration, when the lack of ATP synthesis, and therefore of MMP dissipation, induces significant MMP increase in the three cell types. At least three biological replicates per line: NPC_Ctrl (NI H1, NI H9, NI TFBJ, NI TFC1), NPC_ATP6 (NI A1, NI A2, NI A3), Fib_Ctrl (F20, F30, EF10), Fib_ATP6 (A1, A2, A3), Cyb_Ctrl (TFSR and 143B+), and Cyb_ATP6 (F06, F07, F08). *=$p<0.05$, **= $p<0.01$. **(D)** Treating all cell types with 1 µM oligomycin for 30 min was sufficient to elicit an elevation of the MMP. Values are represented for each cell type in relation to their untreated values. NPC_Ctrl (NI H1, NI TFC2, NI O3, NI O6), NPC_ATP6 (NI A1, NI A2, NI A3), Fib_Ctrl (BJ, LR, Con1), Fib_ATP6 (A1, A2, A3), Cyb_Ctrl (143B+, TFSR), and Cyb_ATP6 (F06, F07, F08). **(E)** Representative images captured using the 96-well plate HCS microscopy Cellomics ArrayScan after four weeks of neuronal differentiation of Neur_ATP6 (from lines NI A2 and NI A3). The HCS images were employed to calculate the percentage of TUJ1 expression in Fig. 5D. **(F)** Imaging-based MMP quantification in individual patient and control neurons. Related to Fig. 5C. **(G)** Volcano plot (log2 fold change vs. -log10 P-value) showing the expression levels of nuclear genes encoding for mitochondrial complexes in NPC_ATP6 (NI A2, NI A3) compared to NPC_Ctrl (NI H1, NI H9, NI TDBJ5, NI TFBJ) significantly changed if p-value < 0.05. **(H)** Heatmap showing the expression of genes regulating mitochondrial calcium homeostasis in ATP6-NPCs (NI A2, NI A3) as compared to control NPCs (NI H1, NI H9, NI TDBJ5, NI TFBJ). This set of genes was used to generate the cluster graphs in Fig. 6A **(I-J)** Global proteomics analysis of down-regulated pathways and up-regulated pathways in NPC_ATP6 (NI A1, NI A2, NI A3) compared to NPC_Ctrl (NI H1, HI H9, NI TFBJ, NI TFC1). Gene set enrichment analysis (GSEA) identified gene sets based on gene ontology gene set C5 (I) and a combined pathway database C2 (J).

S7. Compound high-content screening (HCS) in NPCs_ATP6. Related to Figure 7.
(A-B) The effect of overnight DMSO concentration on NI A2 cells was assessed by measuring in parallel both cell viability with Hoechst (A) and MMP with TMRE and PicoGreen (B) using Cellomics ArrayScan. Cell viability decreased with 4% DMSO. MMP depolarization occurred as expected in the case of treatment with FCCP + antimycin A (AA). Importantly, this treatment alone did not affect cell viability. On the other hand, MMP depolarization occurred also in cells treated with the high doses of DMSO that reduced cell viability (4% DMSO), indicative of cell death. **(C)** Imaging-based readout of MMP (TMRE/PicoGreen/Hoechst) was performed on 384-well plates using the cell analyzer Cellomics ArrayScan. MMP values for the NPC_Ctrl (NI H1) treated with 0.04% DMSO (blue dot) and the NPC_ATP6 (NI A2) treated with FCCP + antimycin A (green dot) are shown in relation to the MMP values of the NPC_ATP6 (NI A2) treated with 0.04% DMSO (orange dot). **(D)** Assessment of cell viability during the compound screening. Values represent the average of the two biological plates each with two technical replicates. Compounds leading to significantly decreased viability

(yellow circles) were excluded from further analysis. Treatment with avanafil did not affect cell viability (arrow).The orange dotted line shows the Hoechst staining value of DMSO-treated NPC_ATP6 (line NI A2) treated with 0.04 % DMSO; the black dotted lines indicate the ±2 SD values. **(E-F)** MMP quantification in permeabilized cells using the Nernst law to express the potential in mV; ADP= state 3 respiration induced by 1 mM ADP; oligomycin= state 4 respiration induced by 1 µM oligomycin. MMP values in NPC_Ctrl (NI TDBJ5, NI TFBJ, NI TFLR, NI TFC1, NI H1) and NPC_ATP6 (NI A1, NI A2, NI A3) treated overnight with avanafil are expressed in relation to MMP values of the untreated cells (at least three biological replicates per line). **(G)** ATP production in individual NPC_ATP6 lines treated with avanafil. Related to Fig. 7C. **(H)** ATP content in individual Neur_ATP6 lines treated with avanafil. Related to Fig. 7D. **(I)** Calcium response in individual Neur_ATP6 lines treated with avanafil. Related to Fig. 7J. **(J)** Schematic representation of the proposed personalized phenotypic drug discovery approach for patients affected by neurological mitochondrial disorders.

Supplemental tables and videos

Table S1. Related to Figure 1 and Figure 7. Transcriptional analysis (tabs 1-5: comparison between NI NPCs and rNPCs and eNPCs; tabs 6-9: comparison between NPC_ATP6 and NPC_Ctrl).

Table S2. Related to Figure 3. Whole mtDNA sequencing.

Table S3. Related to Figure 7. List of compounds used in the screening.

Table S4. Related to STAR Method section. List of PCR primers

Table S5. Related to STAR Method section. List of individuals and cell lines employed in this study.

Video S1. Related to Figure 1. Calcium response in NPC_Ctrl (line NI H1) following glutamate stimulation.

Video S2. Related to Figure 6. Calcium response in NPC_ATP6 (line NI A2) following glutamate stimulation.

Table S4: List of PCR primers

Name	Forward	Reverse
9,932 bp fragment	CCCTCTCTCCTACTCCTG	CAGGTGGTCAAGTATTTATGG
9,506 bp fragment	CTTTATCTGCCTCTTCCTACA CAT CG	GTATGTAGGAGTTGAAGATTAGTCCGCC
PDK1	ACTTCGGATCAGTGAATGCTTG	ACTCTTGCCGCAGAAACATAAA
GLUT3	CGTCGGACTCTTCGTCAACC	GCAGGAAGGATGGTAAAACCC
NANOG	CCTGTGATTTGTGGGCCTG	GACAGTCTCCGTGTGAGGCAT
SOX2	GTATCAGGAGTTGTCAAGGCAGAG	TCCTAGTCTTAAAGAGGCAGCAAAC
NCAM1	TCATGTGCATTGCGGTCAAC	ACGATGGGCTCCTTGGACTC
VIM	GGAGCTGCAGGAGCTGAATG	GACTTGCCTTGGCCCTTGAG
GDF3	TTGGCACAAGTGGATCATTGC	TTGGCACAAGTGGATCATTGC
DPPA4	TGGTGTCAGGTGGTGTGTGG	CCAGGCTTGACCAGCATGAA
DNMT3B	GCTCACAGGGCCCGATACTT	GCAGTCCTGCAGCTCGAGTTTA
ACTB	TCAAGATCATTGCTCCTCCTGAG	ACATCTGCTGGAAGGTGGACA
GAPDH	CTGGTAAAGTGGATATTGTTGCCAT	TGGAATCATATTGGAACATGTAAACC
12S (mtDNA)	TAGCCCTAAACCTCAACA GT	TGCGCTTACTTTGTAGCCTTCAT
28S (nuclear DNA)	ATCCTTCGATGTCGGC	AGCACATACACCAAATGTCT
MT-ATP6	ATCCAAGCCTACGTTTTCAC	CTGTTAGGGGTCATGGGCTGG
D21S2055	AACAGAACCAATAGGCTATCTATC	TACAGTAAATCACTTGGTAGGAGA
DS17S1290	GCAACAGAGCAAGACTGTC	GGAAACAGTTAAATGGCCAA
oriP	TTCCACGAGGGTAGTGAACC	TCGGGGGTGTTAGAGACAAC
D-loop	FAM-GCCACTTTCCACACAGACATCATA	TTAAAAGTGCATACCGCCAAAAG